PNAS NEXUS

PNAS Nexus, 2025, 4, pgaf061

https://doi.org/10.1093/pnasnexus/pgaf061
Advance access publication 25 February 2025
Research Report

Nitrogen stable isotope fractionation by biological nitrogen fixation reveals cellular nitrogenase is diffusion limited

Eunah Han [a,*], Sebastian H. Kopf [b], Ashley E. Maloney [a,1], Xuyuan Ellen Ai [a], Daniel M. Sigman [a] and Xinning Zhang [a,c,*]

[a]Department of Geosciences, Guyot Hall, Princeton University, Princeton, NJ 08544, USA
[b]Department of Geological Sciences, UCB 399, University of Colorado, Boulder, CO 80309, USA
[c]High Meadows Environmental Institute, Guyot Hall, Princeton University, Princeton, NJ 08544, USA
*To whom correspondence should be addressed: Email: xinningz@princeton.edu (X.Z.); Email: eunahh@princeton.edu (E.H.)
[1]Present address: Department of Geological Sciences, UCB 399, University of Colorado, Boulder, CO 80309, USA.
Edited By Edward Bayer

Abstract

Biological fixation of dinitrogen (N_2), the primary natural source of new bioavailable nitrogen (N) on Earth, is catalyzed by the enzyme nitrogenase through a complex mechanism at its active site metal cofactor. How this reaction functions in cellular environments, including its rate-limiting step, and how enzyme structure affects functioning remain unclear. Here, we investigated cellular N_2 fixation through its N isotope effect ($^{15}\epsilon_{fix}$), measured as the difference between the $^{15}N/^{14}N$ ratios of diazotroph net new fixed N and N_2 substrate. The value of $^{15}\epsilon_{fix}$ underpins N cycle reconstructions and differs between diazotrophs using molybdenum-containing and molybdenum-free nitrogenases. By examining $^{15}\epsilon_{fix}$ for *Azotobacter vinelandii* strains with natural and mutated nitrogenases, we determined if $^{15}\epsilon_{fix}$ reflects enzyme-scale isotope effects and, thus, N_2 use efficiency. Distinct and relatively stable $^{15}\epsilon_{fix}$ values for wild-type molybdenum- and vanadium-nitrogenase isoforms (2.5‰ and 5.8–6.6‰, respectively), despite changing cellular growth rate and electron availability, support $^{15}\epsilon_{fix}$ as a proxy for isoform type among extant nitrogenases. Structural mutation of active site N_2 access altered molybdenum-nitrogenase $^{15}\epsilon_{fix}$ (3.0–6.8‰ for α-70VI mutant). Structure-function and isotopic modeling results indicated cellular N_2 reduction is rate-limited by N_2 diffusion inside nitrogenase due to highly efficient catalysis by the active site cofactor, exemplifying $^{15}\epsilon_{fix}$ as a tool to probe N_2 fixation mechanisms. Diffusion-constrained reactions could reflect structural tradeoffs that protect the oxygen-sensitive cofactor from oxygen inactivation. This suggests that nitrogenase function is optimized for modern oxygenated environments and that pre-Great Oxidative Event nitrogenases were less diffusion-limited and potentially exhibited larger $^{15}\epsilon_{fix}$ values.

Keywords: nitrogenase, nitrogen isotopes, enzyme structure–function relationship, diffusion-limited enzyme

Significance Statement

Nitrogen (N) isotope fractionation by N_2 fixers is applied to study environmental N cycling, but its links to cellular N_2 fixation mechanisms and the structural evolution of nitrogenase have been unclear. Using growth experiments and N isotope modeling, we find that nitrogenase active site structure is a key determinant of fractionation. Nitrogenase N_2 reduction in vivo is limited by N_2 transport within the enzyme, indicating that cellular nitrogenase functions at high catalytic efficiency, which could reflect its structural optimization against inactivation by oxygen following the Great Oxidation Event. Ancient N cycle reconstructions should consider $^{15}\epsilon_{fix}$ variability with nitrogenase catalytic efficiency. The results provide insights on the fundamental cellular biology of nitrogenase, a key enzyme in nature.

Introduction

Nitrogen (N) is required for life and is a limiting nutrient in most environments (1). Biological nitrogen fixation (BNF) by the metalloenzyme nitrogenase is the only natural process that can convert abundant but inert dinitrogen (N_2) gas into bioavailable ammonia (NH_3) (Fig. 1a). Investigations of how the strong N≡N triple bond is cleaved under physiological conditions span decades, guiding agricultural and chemical production efforts (5). In vitro studies of nitrogenase biochemistry show that it reduces N_2 by achieving a highly reduced state through a complex sequence of electron transfers to the active site cofactor (Fig. 1b and c) (6, 7). Compared to its in vitro function, in vivo nitrogenase function is subject to additional

Competing Interest: The authors declare no competing interests.
Received: July 10, 2024. **Accepted:** January 21, 2025

influences, including external N_2 transport across the cell envelope and its functional integration with metabolism (8–10). How the nitrogenase reaction functions in cellular environments, particularly its rate-limiting step, are unclear. Identifying the in vivo rate-limiting step is required to understand relationships between nitrogenase structure, mechanism, and cellular physiology, information critical to constraining the ecophysiology and evolution of nitrogen fixers.

Stable isotopes probe diverse chemical processes, ranging from enzymatic reaction mechanism to biogeochemical cycling (11, 12). Knowledge of environmental BNF and its role in present and past N cycling relies on estimates of N stable isotopic ($^{15}N/^{14}N$) fractionation by diazotrophs (1, 13, 14). This fractionation, or "isotope effect" $^{15}\epsilon_{fix}$, is nominally attributed to BNF and can be measured from the $^{15}N/^{14}N$ (or $\delta^{15}N$) difference between dissolved N_2 and newly fixed N (i.e. as an excellent approximation, $^{15}\varepsilon_{fix} = \delta^{15}N_{dissolvedN2} - \delta^{15}N_{newlyfixedN}$, where $\delta^{15}N_{dissolvedN2} = \delta^{15}N_{airN2} + 0.7‰$, newly fixed N is in the form of biomass and excreted N) (12, 15). The mechanisms underlying in vivo $^{15}\epsilon_{fix}$, which can range from 0 to 8‰, are unknown but have been linked to nitrogenase structure and reaction kinetics (Data S2) (8, 16).

The best studied form of nitrogenase uses an iron-molybdenum cofactor in the active site and is more efficient and prevalent than later-evolved alternative isoforms that contain vanadium (V) or iron (Fe) instead of molybdenum (Mo) (17–21). Compared to the Mo isoform, alternative nitrogenases are typically slower at N_2 reduction and have suboptimal active site structure (21), although all nitrogenases are thought to use the same basic mechanisms (2). Values of $^{15}\epsilon_{fix}$ are low for diazotrophs using Mo-nitrogenase (0–3‰) and slightly higher (4–8‰) for V-, Fe-only, and uncharacterized nitrogenases (Data S2) (16, 22–25). Isoform-dependent relationships of in vivo $^{15}\epsilon_{fix}$ with N_2 reduction rate suggest a possible kinetic basis for $^{15}\epsilon_{fix}$ (16, 22, 23, 25). A significantly larger fractionation for purified Mo-nitrogenase has been observed relative to that of cellular nitrogenase (17‰ in vitro vs. 2‰ in vivo) (8, 26). An even larger fractionation (27‰) has been estimated for the chemical reduction of N_2 to 2N2H (HN=NH or N=NH2), a reaction analog of a key BNF step (27). Reconciling these results requires quantitative evaluation of $^{15}\epsilon_{fix}$ informed by nitrogenase reaction mechanism. Mechanistic evaluations of $^{15}\epsilon_{fix}$ could also provide new insights into nitrogenase reaction kinetics (3, 8, 16, 23), since net isotopic fractionation is generally controlled by the rate-limiting step of a reaction network (11, 28).

Here, we aim to decipher the mechanisms of N isotopic fractionation for BNF by *Azotobacter vinelandii*, a unicellular diazotroph used in seminal studies of BNF physiology and biochemistry (7, 29). We propose mechanisms underlying $^{15}\epsilon_{fix}$ based on cellular N isotope dynamics, then examine the $^{15}\epsilon_{fix}$ and physiology of diazotrophic strains using structurally different wild-type or mutant nitrogenases. To quantitatively interpret the results, we use a N isotope model of $^{15}\epsilon_{fix}$ informed by nitrogenase reaction mechanism. We find that enzymatic isotope effects are the origin of cell-level fractionation. Small $^{15}\epsilon_{fix}$ values indicate rate-limitation by enzymatic N_2 diffusion while larger $^{15}\epsilon_{fix}$ values reflect greater expression of the kinetic isotope effect (KIE) of N_2 catalysis. The results indicate that nitrogenases operate with high catalytic efficiency in vivo, consistent with the optimized cellular functioning of this metabolically expensive enzyme.

Results

Cellular N isotope dynamics for in vivo BNF by *A. vinelandii*

To constrain $^{15}\epsilon_{fix}$, we focus on in vivo BNF by the aerobic unicellular diazotroph *A. vinelandii*, an important organism in nitrogen fixation research (7, 29). We examine the role of isotopically sensitive N_2 transport and catalysis steps in the net reaction sequence starting with atmospheric N_2 gas and ending with fixed N production by nitrogenase (left to right, Fig. 1b). At steady state, $^{15}\epsilon_{fix}$, the observable isotope fractionation of this multistep process, should reflect the KIE of the rate-limiting, N-based step and the equilibrium isotope effects (EIEs) of preceding steps (11, 28), since processes after the rate-limiting step do not affect fractionation (because of complete transformation of subsequent intermediates into the final product) (30, 31). The availability of electrons and other substrates for BNF can indirectly affect $^{15}\epsilon_{fix}$ by influencing the relative rates of N-based reaction steps.

Dissolution of N_2 in air into the aqueous extracellular matrix (Fig. 1b, leftmost blue arrow) is not expected to constrain $^{15}\epsilon_{fix}$ since it is not rate-limiting. High N_2 partial pressure in air (0.79 atm) relative to the dissolved N_2 concentration at saturation (<20 ppm (32)) leads to a dynamic equilibrium that is expressed as a small EIE, 0.7‰ (15, 32). In contrast, N_2 diffusion through the cell envelope and cytosol to nitrogenase, can determine $^{15}\epsilon_{fix}$ if it constrains N_2 reduction by nitrogenase (Fig. 1b, green). Since substrate diffusion/uptake by cells is generally not a highly fractionating process (30, 33, 34), a "Cellular Reservoir" hypothesis has been proposed (8). This hypothesis maintains that when cytosolic N_2 is limited, the large KIE expected for nitrogenase is incompletely expressed (Fig. 1b, green), leading to small $^{15}\epsilon_{fix}$ values expected for N_2 transport into a cell. Low cellular $^{15}\epsilon_{fix}$ values for diazotrophs using Mo-nitrogenase would result from significant depletion of the cellular N_2 reservoir by this isoform. Slightly larger $^{15}\epsilon_{fix}$ values associated with alternative nitrogenases might then result from their slower N_2 reduction and lower degree of cytosolic N_2 limitation.

Enzymatic reaction steps shape $^{15}\epsilon_{fix}$ if nitrogenase reaction kinetics control in vivo BNF rate. The isotopically sensitive enzymatic reaction steps comprise cytosolic N_2 diffusion through the substrate channel of nitrogenase to its active site ("enzymatic N_2 diffusion," Fig. 1b, orange) and N_2 catalysis, which includes N≡N binding to the active site cofactor and triple bond breaking (Fig. 1b, catalysis box) (6). Net enzymatic fractionation (equivalent to $^{15}\epsilon_{fix}$ if cytosolic N_2 is not limiting) should respond to the relative importance of enzymatic N_2 diffusion vs. catalysis for N_2 reduction rate, which is influenced by electron transfer to the active site cofactor (29, 35).

The Thorneley–Lowe kinetic scheme is a long-standing model for substrate-cofactor interactions that indicates that the resting state cofactor (E_0) must sequentially accumulate four electrons and four protons to reach a critical E_4-4H state (Fig. 1b) (29, 35). The reduced cofactor is short-lived as it can oxidatively decay, releasing H_2 from hydride protonation (Fig. 1b, lower left) if substrate availability is low (i.e. electrons at E_2, N_2 at E_4, Fig. 1b, lower left to middle). Given sufficient N_2 availability at E_4-4H (Fig. 1b middle), two cofactor-bound hydrides are released as H_2 (reductive elimination), yielding a short-lived E_4-2H cofactor in which the remaining pair of electrons and protons bind N≡N, producing cofactor-bound N_2-2H (6, 29). The bond-breaking reduction of cofactor bound N_2-2H to 2N2H (HN=NH or N=NH2) is generally accepted to be immediate since no additional electron inputs are required (6), but details on the catalytic mechanism remain debated (6, 36–38). Unless H_2 partial pressure at the active site is very high (0.7 atm), N_2 reduction is irreversible (39). Downstream steps (e.g. cofactor bound-2N2H reduction to $2NH_3$) allow the cofactor to complete its redox cycle back to E_0, with NH_3 release into the cytosol (Fig. 1b). These dynamics suggest that enzymatic fractionation is constrained by reaction steps

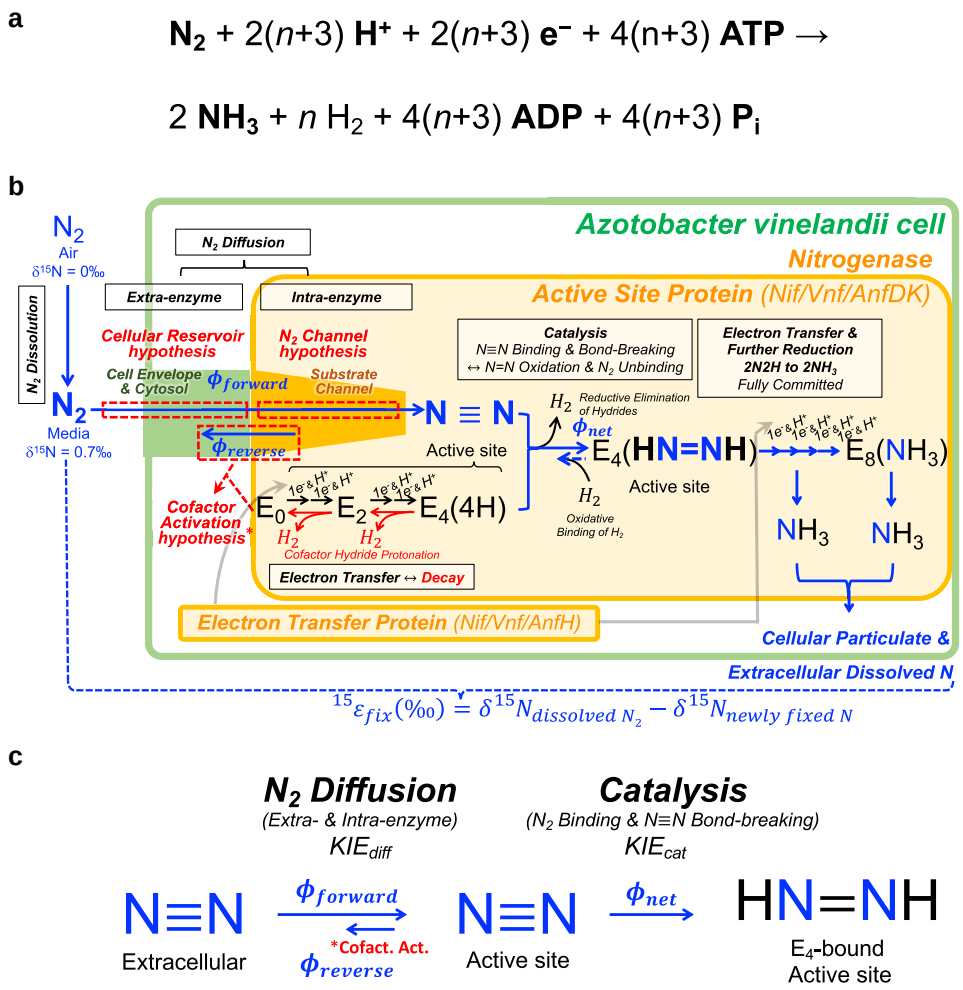

Fig. 1. In vivo N_2 reduction by *A. vinelandii* nitrogenase. a) Nitrogenase reaction requires protons (H^+) and electrons (e^-) to reduce 1 mol N_2 to 2 mol NH_3 and *n* mol dihydrogen (H_2). Since N_2 binding necessitates H_2 release at the active site cofactor, $n \geq 1$ and varies by reaction condition and Mo- (*Nif*), V- (*Vnf*), Fe-only (*Anf*) isozyme type (2–4). 2ATP are hydrolyzed to 2ADP and inorganic phosphate (P_i) for each electron transferred between Fe-proteins (*NifH*/*AnfH*/*AnfH*) and active site proteins (*NifDK*/*VnfDK*/*AnfDK*). b) Reaction scheme for cellular N_2 fixation by nitrogenase. N_2 transport steps (dissolution, extra- and intraenzyme diffusion, left of diagram) to the active site precede catalysis (middle to right diagram). Parallel to intraenzyme N_2 diffusion, cofactor accumulation of $4e^-$ from nitrogenase Fe-proteins (bottom left of diagram) results in cofactor activation for catalysis (E_4 stage cofactor). Net N isotope fractionation for cellular BNF ($^{15}\epsilon_{fix}$) is constrained by rate-limiting, N-involving steps (blue) and their isotope effects. Possible mechanisms for $^{15}\epsilon_{fix}$ focus on N_2 dynamics in the cellular reservoir and active site. The $\delta^{15}N$ of newly fixed N is calculated using the $\delta^{15}N$ and N quotas of particulate (biomass) and dissolved (excreted) N pools (see Materials and methods, Data S1). c) Simplified reaction scheme of cellular N_2 fixation and key isotope effects. The reversibility of N_2 diffusion may be affected by slow cofactor activation (*, Cofactor Activation hypothesis, Fig. 1b).

preceding N_2 catalysis, since this step is likely irreversible under in vivo conditions (e.g. $pH_2 < 0.7$ atm).

When enzymatic N_2 diffusion is slower than electron transfer to the cofactor, we suggest that the expression of a larger KIE of catalysis is masked ("N_2 Channel" hypothesis, Fig. 1b, orange) (30, 31, 40). Under this fast electron transfer condition, active site N_2 molecules mainly encounter the cofactor at E_4 state (41–43) and proceed to catalysis. This results in limited diffusional loss of N_2 from the nitrogenase active site to the enzyme's exterior environment. Consequently, enzymatic fractionation would converge on the KIE of the slow enzymatic diffusion step, which is expected to be relatively small compared to that of catalysis (11). This hypothesis predicts that, under high cellular N_2 availability, the highly efficient redox cycling of the cofactor leads to N_2 channel diffusion becoming the rate-limiting step of in vivo BNF (29, 35), resulting in small cell-scale $^{15}\epsilon_{fix}$ values.

Conversely, slow electron transfer to the cofactor could lead to more reversible N_2 diffusion as N_2 is less likely to encounter the E_4 cofactor ("Cofactor Activation" hypothesis, Fig. 1b) (35, 44), such that $^{15}\epsilon_{fix}$ shifts towards the expression of the larger KIE of the downstream catalysis step. This hypothesis predicts an increase in $^{15}\epsilon_{fix}$ with lower electron availability and nitrogenase N_2:H_2 ratios (the molar ratios of reduced N_2 to produced H_2 from cofactor decay). Specifically, it suggests that the lower $^{15}\epsilon_{fix}$ and N_2:H_2 ratios associated with Mo-nitrogenase compared to alternative nitrogenases are derived from this isoform's higher electron use efficiency for NH_3 production, which results from its increased commitment toward N_2 catalysis (Fig. 1b) (16).

Many in vitro studies, including Thorneley and Lowe (1983), have reported electron transfer from Fe-protein to MoFe-protein (lower left, Fig. 1b), or consequent cofactor activation from E_0 to E_4, as the rate-limiting step for in vitro Mo-nitrogenase reaction (35, 44, 45). Harris et al. (37) recently showed N≡N bond breaking to be a previously overlooked slow step for in vitro BNF under fast electron transfer conditions. How electron and N dynamics play out in vitro and in vivo environments and link to $^{15}\epsilon_{fix}$ is unclear.

Diazotrophic cultures of *A. vinelandii*

To determine the role of nitrogenase enzyme characteristics and cellular physiology on $^{15}\epsilon_{fix}$, we grew 13 strains of *A. vinelandii* utilizing either the wild-type Mo-nitrogenase (WT), wild-type V-nitrogenase (V-only), or artificially mutated Mo-nitrogenase under diazotrophic conditions in batch and chemostat cultures. Mutant strains with alterations in the *NifDK* active site protein (6, 29, 46) or gene deletion for the primary physiological electron donor to nitrogenase, *NifF* (10), used to define the BNF reaction mechanism (Table 1). Based on prior findings, we classified *nif* mutations into four functional groups: gate keepers of N_2 substrate channeling (strains Na1, Na2, Nb, NbE, NbH), proton transfer (Ha, Hb, NbH), electron transfer (Ea, Eb, NbE), or transition state stabilization (T) at the active site in the MoFe-protein (Table 1, Fig. S1, Supplementary Materials and methods S1.1) (6, 58–60).

We grew all strains in batch culture to examine $^{15}\epsilon_{fix}$ under conditions of maximum diazotrophic growth and a subset of the strains (WT, V-only, Na1, Na2) at slow growth rates in chemostat cultures (0.6 and 2 d^{-1} < all batch growth rates) (61, 62). We assessed the effect of N_2 partial pressure by using higher levels in chemostat (0.97 atm pN_2) than in batch culture (0.79 atm pN_2 in air) (63, 64) and of electron availability by comparing electron-replete batch cultures with high medium carbon (2% glucose and mannitol) and high headspace O_2 (0.21 atm in air) to electron-limited chemostat cultures with low availability of carbon (0.15% sucrose) and O_2 (0.03 atm) (63, 64) (see Supplementary Materials and methods S1.2 and S1.5). We measured $^{15}\epsilon_{fix}$ for all culture experiments, cell density and growth rate (μ) for all batch cultures, and specific activity per MoFe-protein for all Mo-nitrogenase strains (Figs. 2 and 3, Data S1).

Enzymatic basis of A. vinelandii *cellular* $^{15}\epsilon_{fix}$

The WT strain grew faster than all other batch cultured strains (5.3 ± 0.1 d^{-1}, mean ± 1 SD) and exhibited small, stable cellular $^{15}\epsilon_{fix}$ values (2.5 ± 0.0‰, Fig. 2, Data S1) for both fast batch culture growth and slower chemostat growth (0.6 and 2 d^{-1}). V-only batch cultures grew more slowly (3.9 ± 0.1 d^{-1}) and expressed larger $^{15}\epsilon_{fix}$ values (6.6 ± 0.1‰). V-only $^{15}\epsilon_{fix}$ slightly decreased for slow chemostat growth (5.8 ± 0.2‰ and 6.1 ± 0.2‰ at μ = 0.6 and 2 d^{-1} respectively). These results are consistent with growth rate and $^{15}\epsilon_{fix}$ data from previous studies (16, 23, 62).

Batch growth of each *nif* mutant was slower than for the WT strain, confirming the negative effect of mutations on diazotrophy (Table 1, Figs. 2 and 3a). Values of $^{15}\epsilon_{fix}$ for the majority of mutants were only slightly higher than for the WT (≤1‰ increase in $^{15}\epsilon_{fix}$ for 9 of 11 strains, Data S1). Certain substrate channel mutants with altered N_2 diffusion and binding (Na1, Nb, and NbE strains) exhibited higher values ($^{15}\epsilon_{fix}$ = 4.1–6.8‰). We excluded alternative nitrogenase activity as a cause of higher $^{15}\epsilon_{fix}$ for the Na1 mutant (Table S2, Supplementary Materials and methods S1.4).

These results rule out a low flux of external N_2 to nitrogenase as an important constraint on *A. vinelandii* cellular $^{15}\epsilon_{fix}$ (Cellular Reservoir hypothesis, Fig. 1b). Cellular N_2 reservoir control on $^{15}\epsilon_{fix}$ should result in covariation of $^{15}\epsilon_{fix}$ with diazotrophic μ, cell density, and protein levels when external N_2 limits nitrogenase. In contrast, we found no global correlation between $^{15}\epsilon_{fix}$ and μ across strains and culture methods (black bars or symbols, Figs. 2 and 3a), consistent with prior studies (16, 23). Additionally, $^{15}\epsilon_{fix}$ remained constant with cell density in batch cultures (Fig. 3b) and did not vary with protein specific activity (Fig. 3f).

The results demonstrate the enzymatic basis of cellular $^{15}\epsilon_{fix}$, specifically, the pivotal role of nitrogenase structure in governing this parameter. This interpretation is consistent with an inferred enzymatic $^{15}\epsilon_{fix}$ value of ~2.5‰ for the WT Mo nitrogenase of *Anabaena*, a heterocystous multicellular diazotroph, using interpolation of cellular $^{15}\epsilon_{fix}$ data under different headspace pN_2 levels (9). Importantly, the finding of large $^{15}\epsilon_{fix}$ for the *nif* mutant Na1 equivalent to that of the V-only strain due to substrate channel mutation demonstrates that the FeMo-cofactor by itself does not control enzymatic $^{15}\epsilon_{fix}$ (16, 22). Instead, the data suggest that cofactor and substrate interactions constrained by nitrogenase structure are key controls of enzymatic $^{15}\epsilon_{fix}$.

N isotope model of BNF

To quantitatively interpret $^{15}\epsilon_{fix}$ as a function of the intraenzyme steps of the nitrogenase reaction, we constructed a steady state N isotope model of the net isotope effect for BNF, $\alpha_{fix} = 1 + (^{15}\varepsilon_{fix}/1,000)$, (Fig. 4) based on the Thorneley–Lowe kinetic scheme for cofactor N_2 reduction to NH_3 (Fig. 1b) (35), N flux ratios (*f* in Fig. 4a–c), and experimentally or theoretically determined isotope effects. Biochemical observations and chemical theory enabled simplification of the nitrogenase reaction mechanism (Fig. 1b into c) into two steps, reversible N_2 diffusion step followed by irreversible N≡N catalysis (top panel of Fig. 4, see Materials and methods). To investigate the role of different flux ratios at those enzymatic steps, we formulated the model in three interconvertible forms:

$$\alpha_{fix} = -(KIE_{cat} - KIE_{diff}) \cdot f_{used} + KIE_{cat} \quad (1)$$

$$\alpha_{fix} = (KIE_{cat} - KIE_{diff}) \cdot f_{diff} + KIE_{diff} \quad (2)$$

$$\alpha_{fix} = \frac{(KIE_{diff} \cdot f_{ctc}) + KIE_{cat}}{f_{ctc} + 1}. \quad (3)$$

With ϕ referring to fluxes of N_2, flux ratio $f_{used} = \phi_{net}/\phi_{forward}$ ranging from 0 to 1 represents the nitrogenase catalytic demand for N_2 substrate relative to the supply entering the active site (i.e. N_2 use efficiency) (28); $f_{ctc} = \phi_{net}/\phi_{reverse}$ ranging from 0 to ∞ is the commitment to catalysis (30); $f_{diff} = \phi_{reverse}/\phi_{forward}$ ranging from 0 to 1 is the reversibility of N_2 diffusion (65). Terms KIE_{diff} and KIE_{cat} denote the forward kinetic isotope effects of N_2 diffusion and of N_2 catalysis, respectively. The flux ratios constrain $^{15}\epsilon_{fix}$ by dictating where the rate-limiting step of the BNF reaction sequence occurs and thus the contributions of KIE_{diff} and KIE_{cat} to $^{15}\epsilon_{fix}$.

The magnitudes of KIE_{diff} and KIE_{cat} have not been empirically determined. We estimated possible values for KIE_{diff} (from 1 to 1.0068, i.e. ϵ_{diff} from 0 to 6.8‰) based on the physical chemistry of molecular diffusion (KIE_{diff} in air = 1.0089, KIE_{diff} in water = 1.0068) (66). KIE_{cat} is comprised of the KIE for N_2 binding to the cofactor and the KIE of N≡N bond cleavage to 2N2H, which Herzberg (1945, 1950) calculated to be 1.027 (i.e. ϵ of cleavage = 27‰) based on N_2 vibrational frequencies (27, 67, 68). The KIE of N_2 cofactor binding is poorly constrained (41, 42), as the binding mode remains unclear (see Supplementary Results S1.8). To account for possible normal or inverse binding isotope effects (69), we assume that the binding KIE modulates KIE_{cat} so as to cause it to range between 1.017 and 1.037 (i.e. ϵ_{cat} from 17 to 37‰). The above chemical KIEs represent maximum possible values for the intrinsic enzymatic KIE (5, 70). We calculated the equilibrium isotope effect (EIE) for chemical N≡N bond cleavage to 2N2H (E_4 forward arrow, Fig. 1b) to be 1.065 based on the vibrational bond energies (R Code S1) (71, 72), which indicates

Table 1. Description of *A. vinelandii* strains using wild-type nitrogenases or Mo-nitrogenase (*nif*) mutant enzymes and homologous proteins.

Code	Strain	Mutation	Function		In vitro kinetics[a]			Active site		
			Residue function or mutation effect	Confirmation residue function?	NH_3	H_2	K_m	Gate keeper	Catalytic center	Gate width
***Azotobacter vinelandii*, Mo-nitrogenase**										
WT	DJ995		Wild type		600	640	0.1–0.2 atm N_2	α-70 Val	Fe6 of FeMo-co	0.45 nm
					590	690				
					891	578				
N_2 substrate access Mo-nitrogenase mutants										
Na1	DJ1373	α-70VI	Gatekeeper (narrower N_2 gate)	Confirmed	170	1940	>1.5 atm N_2	α-70 Ile	Fe6 of FeMo-co	0.38 nm
Na2	DJ1310	α-70VA	Gatekeeper (wider N_2 gate)	Confirmed	360	1440		α-70 Ala	Fe6 of FeMo-co	0.55 nm
Nb	DJ1262	α-69GS	Gatekeeper's neighbor (sensitive to C_2H_2)	Confirmed	810					
NbH	DJ1269	α-69GS and α-381FL	Gatekeeper's neighbor (insensitive to C_2H_2)	Confirmed	ND					
NbE	DJ1270	α-69GS and β-98YH	Gatekeeper's neighbor (insensitive to C_2H_2)	Confirmed	ND					
Nc	DJ776	α-191QP	Gatekeeper's neighbor (wider N_2 gate)	Confirmed	ND					
Proton path Mo-nitrogenase mutants										
Ha	DJ948	α-440QN	Altered proton channel Mimicking alternative nitrogenases (Q to N)	Putative	ND					
Hb	DJ124	α-276YS	Altered proton transfer to a S atom of FeMo-co	Putative	ND					
Electron supply Mo-nitrogenase mutants										
Ea	DJ60	*ΔnifF*	Flavodoxin gene deletion	Confirmed	ND					
Eb	DJ63	α-161DE	Altered electron transfer to FeMo-co	Confirmed	ND					
Transition state Mo-nitrogenase mutant										
T	DJ1266	α-96RK	Different transition state Similar to alternative nitrogenase (R to K)	Confirmed	ND					
***Azotobacter vinelandii*, V-nitrogenase**										
V-only	CA11.70	Mo-, Fe-nitrogenase deletion	Wild type (ΔnifHDK ΔanfHD70::kan)	411	711	0.3 atm N_2	V-only	α-57 Val	Fe6 of FeV-co	0.45 nm
Azotobacter vinelandii*, *NifE										
			Homologous to *NifDK*					α-45 Ala	Fe6 of L-cluster	1.33 nm
***Methanosarcina acetivorans*, F_{430} (*NflD*)**										
			Homologous to *NifDK*					α-19 Ala		ND
***Rhodobacter capsulatus*, Bacteriochlorophyll**										
			Homologous to *NifDK*					β-274 Asp	Mg	0.94 nm

Kinetics of purified enzymes[a] at 1 atm N_2 in units of $\mu mol_{NH3\ or\ H2} \cdot min^{-1} \cdot g_{MoFeP}$ or $^{-1}_{VFeP}$. Molecular weight of MoFe-protein ($NifD_2K_2$) is 230 kDa and of VFe-protein ($VnfD_2K_2$) is 270 kDa (18). K_m is the Michaelis–Menten constant (4, 47–51). Substrate channel gate width in protein homologs of *NifDK* were estimated from X-ray crystallography files (1M1N, 3K1A, 6FEA, 3PDI, 3AEK) using PyMOL v2.5.5 (52–57). Additional strain information in Supplementary Materials and methods.

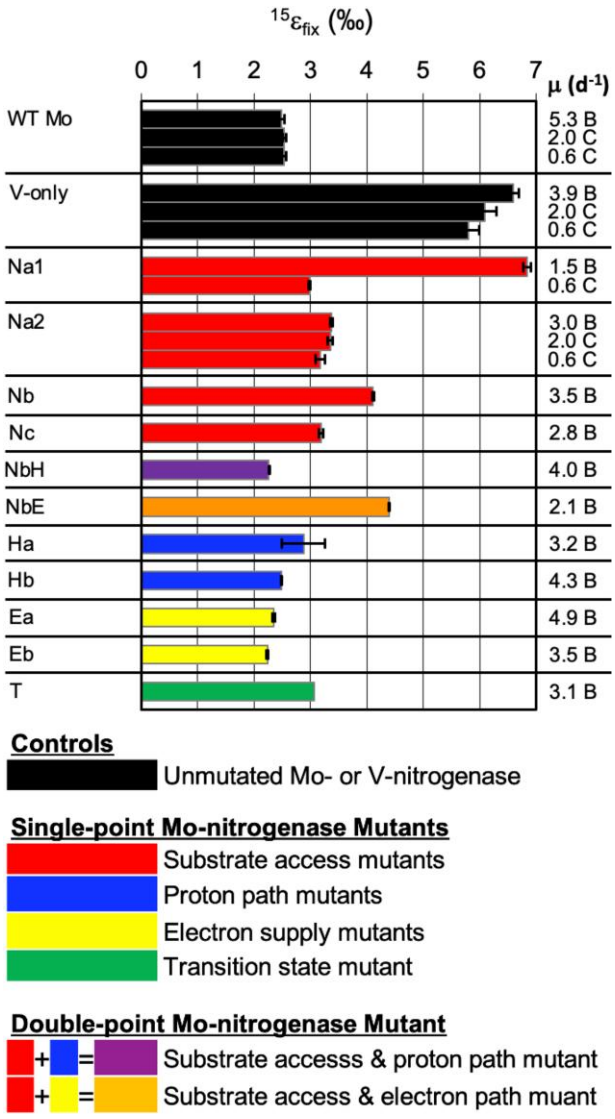

Fig. 2. Cellular $^{15}\epsilon_{fix}$ and growth rate of *A. vinelandii Using Natural Mo-, V-, or Artificially Mutated Mo-nitrogenase for Diazotrophy*. Nitrogenase type is denoted by bar color (see legend below); see detailed strain descriptions in Table 1. The right column shows growth rate (μ) and growth condition (batch or chemostat denoted by "B" or "C" letters, respectively.

that reversible catalysis would lead to observed $^{15}\epsilon_{fix}$ between 27 and 65‰. As measured $^{15}\epsilon_{fix}$ values are always much lower in amplitude, they do not support reversible catalysis (Supplementary Results S1.9).

Modeled KIEs and flux ratios for $^{15}\epsilon_{fix}$ reveal variable nitrogenase function

We calculated all best-fit values of KIE_{diff}, KIE_{cat}, and f for each $^{15}\epsilon_{fix}$ observation (Table S1 and Fig. S1, Supplementary Code R2). The range of f ratios in Fig. 4 represents conditions spanning maximum and minimum enzyme function for NH_3 production (N_2 use efficiency, closed vs. open circles in Fig. 4d and e). In the case of maximum enzyme function, enzymatic N_2 diffusion strongly constrains net rate, and measured $^{15}\epsilon_{fix}$ converges on the relatively small fractionation ϵ_{diff} (0 to 6.8‰) due to KIE_{diff} (1 to 1.0068). Net rate for poor enzymatic function is more strongly affected by N≡N catalysis, and $^{15}\epsilon_{fix}$ reflects the fractionation due to KIE_{cat} alone (for α_{fix}≈1.027 and 1.037, $^{15}\epsilon_{fix}$≈27 and 37‰, when f_{used} and f_{ctc} approach zero, see Eqs. (1) to (3)).

Nitrogenase N_2 uses efficiency, which is represented by f_{used} (Figs. 4d and e, Table S1), varied substantially between in vivo and in vitro reaction conditions (1 and 0.4, respectively) but was less sensitive to enzyme structure and growth condition (≥ 0.8). Notably, the high in vivo f_{used} values indicate that nitrogenases operate at intermediate to high efficiency under cellular settings. The results demonstrate the critical importance of reaction setting, and the optimized function of nitrogenase in a cellular environment.

Overall, the data indicate that the wild-type Mo-nitrogenase represents the "best" nitrogenase structure as its cellular function remained very high across all growth conditions, at the highest possible ranges of f_{used} and f_{ctc}. Functioning of wild-type V-enzyme and mutant Mo-nitrogenases was not as high as WT Mo-nitrogenase. Functional defects were most apparent in N_2 substrate channel mutants (e.g. Na1 strain) and could vary with its growth physiology.

Wild-type Mo-nitrogenase $^{15}\epsilon_{fix}$: near perfect catalysis in cellular environments

The low and stable $^{15}\epsilon_{fix}$ values for the wild-type Mo-nitrogenase indicating N_2 use efficiency near unity imply that this enzyme achieves very high in vivo turnover relative to enzymatic N_2 diffusion across varying electron availability conditions. This functional state may reflect this enzyme's optimized cofactor and amino acid environment in the active site and meets the definition of "catalytic perfection" proposed by Knowles and Albery (43) in which all encounters between enzyme and substrate result in conversion to product. Indeed, this interpretation is supported by our kinetic calculations. The in vitro k_{cat}/K_m≥1.4×10^5/s/M (Supplementary Results S2.3). The high in vitro $^{15}\epsilon_{fix}$ of 17‰ could reflect less efficient electron transfer to the cofactor than in vivo. This could result from artificial reaction conditions that are suboptimal for the enzyme or other factors (e.g. in vitro assay artifacts). The significantly lower cellular $^{15}\epsilon_{fix}$ values must reflect even higher k_{cat}/K_m values (≥10^8/s/M) approaching the magnitude expected for most diffusion-limited enzymes (36, 38).

The operation of nitrogenase at its diffusional limit across all growth conditions implies that diazotrophs maximize the function of active (E_4) nitrogenase, perhaps by managing total MoFe-protein pool size or the distribution across E_n states. If the ratio of active MoFe-protein to total MoFe-protein in a cell ($E_4/\sum_{n=0}^{8} E_n$) changes with reaction condition and enzyme type (see Supplementary Discussion S3.1), then total enzyme measurements may not be directly comparable across conditions (and enzymes).

Nif active site mutants: key gatekeeping amino acids constrain substrate-cofactor interactions and $^{15}\epsilon_{fix}$

Active site mutations affecting N_2 access in Mo-nitrogenase had the largest effects on $^{15}\epsilon_{fix}$, particularly those at the α-70 gatekeeping position for substrate N_2 positioning and selectivity (73–75). A "gatekeeping" residue refers to an amino acid residue(s) that plays a critical role in selecting accessibility of a molecule to the enzyme's catalytic center based on the molecule's size and chemical properties (76). The gatekeeping status of α-70 was elucidated by studies of Na1 (residue α-70V mutated to I), Na2 (α-70VA), Nb (α-69GS), and Nc (α-191QP) (Table 1) (58, 60, 73). The Na1 and Na2 enzymes have suboptimal gate widths due to substitution of α-70 with larger or smaller amino acids, respectively (Table 1),

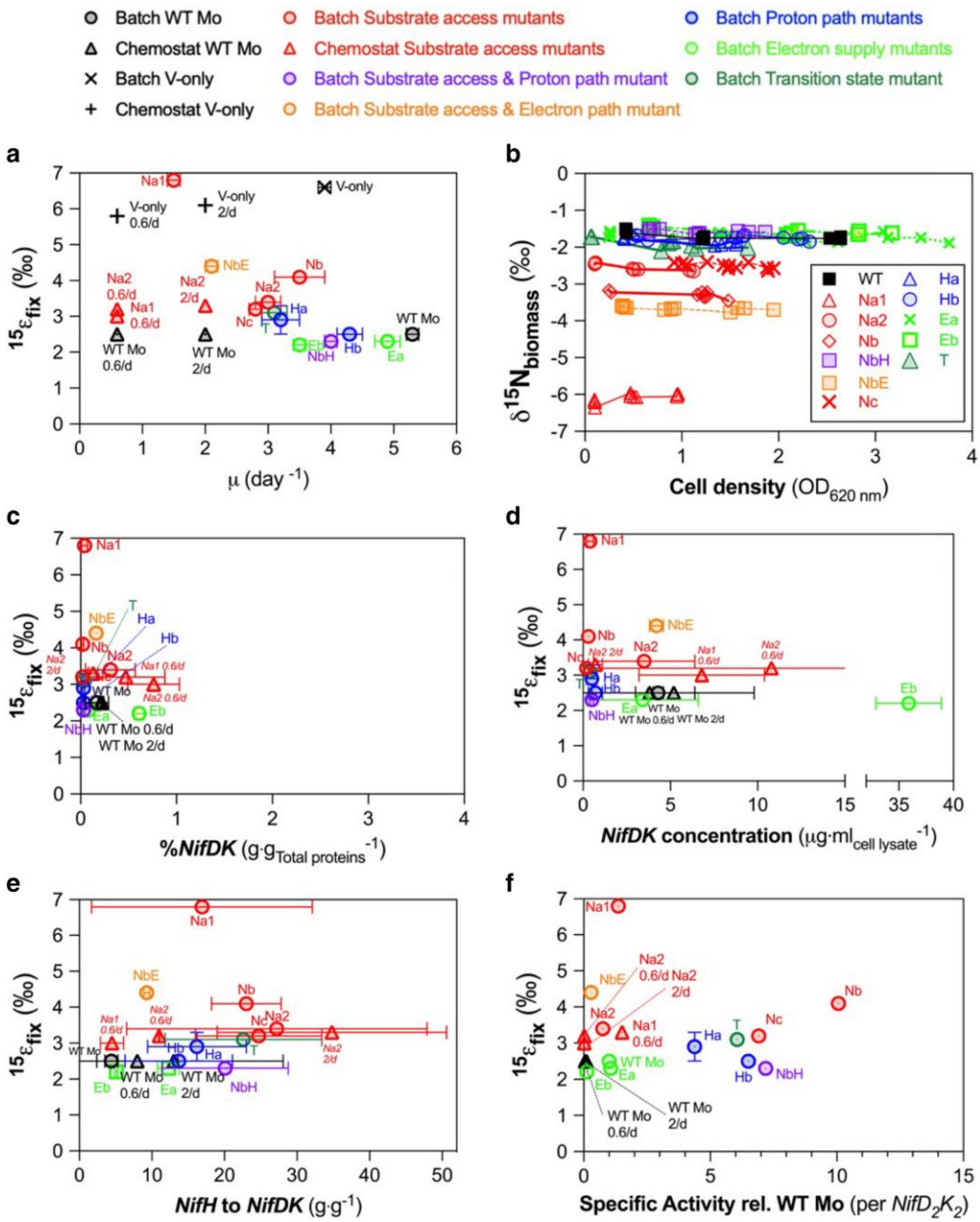

Fig. 3. Absence of correlation between cellular $^{15}\epsilon_{fix}$ and physiology indicates the control of $^{15}\epsilon_{fix}$ by intraenzyme process. The physiological factors measured in our cell cultures include (a) growth rate, (b) cell density, (c) the mass proportion of nitrogenase amongst all intracellular proteins, (d) the concentration of nitrogenase in cell lysate, (e) the mass ratio of Fe-protein to MoFe-protein, and (f) the rate of fixed N accumulation per gram of nitrogenase compared to wild type (WT). The absence of global correlation between cellular $^{15}\epsilon_{fix}$ and physiological metrics indicates an enzymatic basis for $^{15}\epsilon_{fix}$. See Methods for rate calculation in (f). For (b), biomass $\delta^{15}N$ differs from $^{15}\epsilon_{fix}$ by <1‰, indicating a minimal effect of N excretion on $^{15}\epsilon_{fix}$ (see Supplementary Materials and methods).

resulting in less efficient N_2 fixation (much lower N_2:H_2 ratios) (47, 48, 77, 78).

The higher $^{15}\epsilon_{fix}$ relative to WT enzyme for the structurally suboptimal Na1 enzyme for all growth conditions can be explained by the α-70VI mutation disrupting N_2 interactions at the FeMo-cofactor. This leads to more reversible diffusion and decreased commitment to catalysis (Fig. S4d and e). This interpretation is supported by recent findings indicating that the bulky sidechain of the substituting isoleucine in Na1 interrupts N_2 binding to the E_4 cofactor by slowing H_2 elimination (75). This decreases cofactor reactivity, commitment to catalysis, leading to more active site N_2 loss (lower f_{used}) and greater expression of the KIE_{cat} in the $^{15}\epsilon_{fix}$ value. The decrease in Na1 $^{15}\epsilon_{fix}$ between batch and chemostat conditions towards the WT value (6.8 to 3.0‰) indicates that the Na1 mutation effect on cofactor reactivity and substrate use efficiency is modulated by physiological context. Lower cellular electron availability in chemostat cultures may have suppressed E_4 cofactor decay (75), increasing the forward flux ratio for N_2 conversion to NH_3 relative to batch culture conditions (see Supplementary Results S2.1). Overall, the Na1 $^{15}\epsilon_{fix}$ data confirm the critical role of the α-70 residue in optimizing the position of N_2 for high substrate use efficiency at the active site.

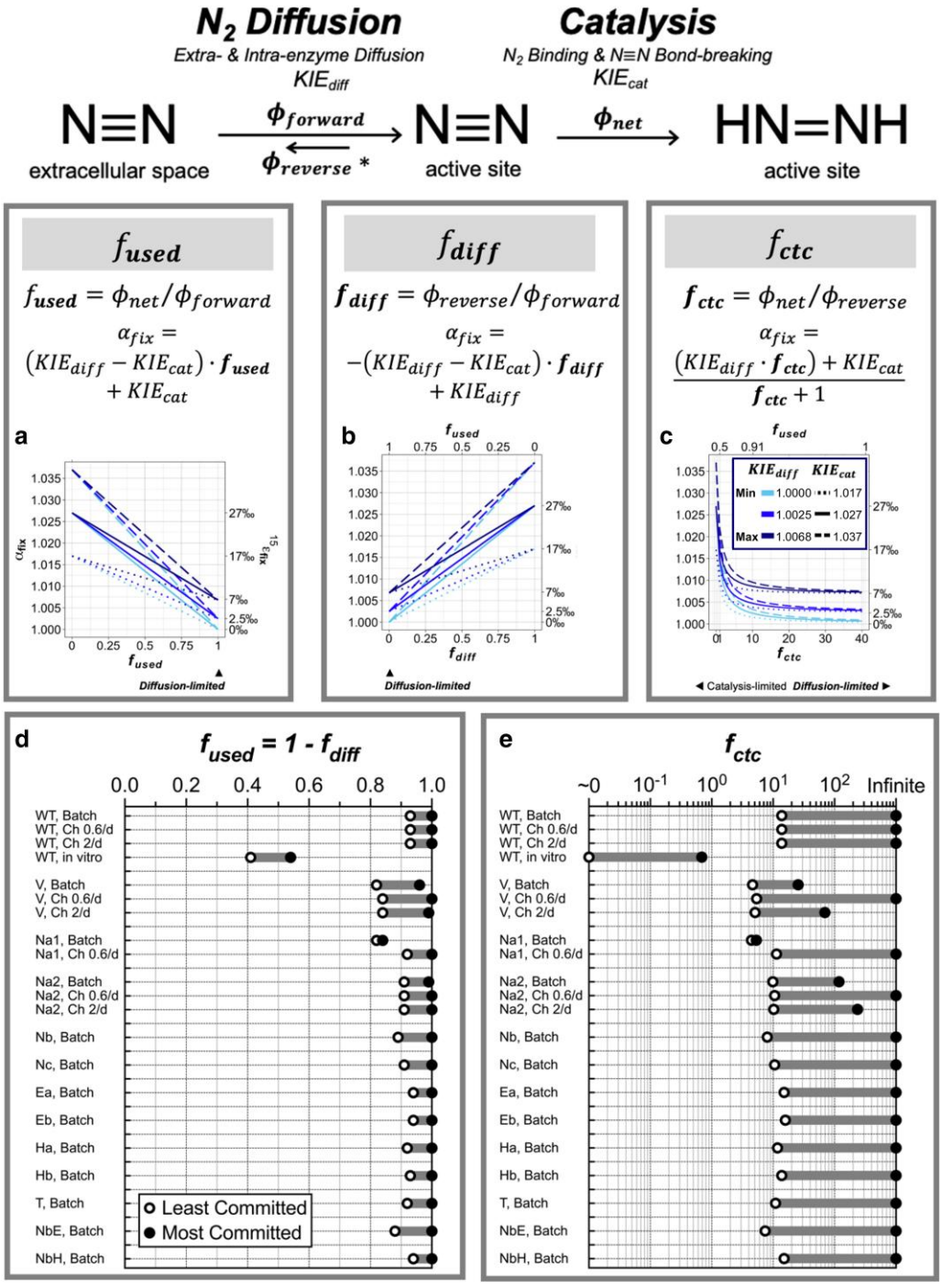

Fig. 4. ^{15}N fractionation model indicates high N_2 use efficiencies for nitrogenases in the cellular environment. BNF ^{15}N dynamics can be simplified (top panel, Fig. 1c) into a steady-state ^{15}N model (middle panels) based on N_2 flux ratios representing (a) nitrogenase N_2 use efficiency, f_{used}; (b) reversibility of N_2 diffusion in nitrogenase, f_{diff}; and (c) commitment to catalysis at the N_2 bind/bond step, f_{ctc}. a–c) Steady state sensitivities of modeled $^{15}\epsilon_{fix}$ to various flux ratios given different model-imposed values (see legend color and line style) for KIE_{diff} and KIE_{cat} are shown. d, e) Best-fit model solutions for the range of flux ratios (dark grey line) complying with measured $^{15}\epsilon_{fix}$ for each nitrogenase strain, given the imposed ranges for KIE_{diff} and KIE_{cat} (Table S1, see Supplementary Materials and methods) are shown. Flux ratios represent each nitrogenase functioning at their highest substrate use efficiency (most committed towards NH_3 production, filled circles) and lowest efficiency (least committed, open circles). WT Mo-nitrogenase in vitro $^{15}\epsilon_{fix}$ is reported in Sra et al. (26), while all other $^{15}\epsilon_{fix}$ values are from this study. Imposed KIE_{diff} values were generally <3‰. See Table S1 and Fig. S1 for details.

In addition to Na1, the higher $^{15}\epsilon_{fix}$ of other substrate access mutants (Na2, Nb, Nc) compared to the WT supports reversibility of enzymatic N_2 diffusion as a key modulator of $^{15}\epsilon_{fix}$. But the smaller isotopic change observed for these enzymes compared to Na1 may indicate weaker mutational effects on cofactor reactivity (Supplementary Results S2.1).

Other *nif* mutations affecting the transition state, electron transfer to or within nitrogenase, or proton pathway led to small or no changes in $^{15}\epsilon_{fix}$ relative to the WT, confirming the critical importance of substrate access for $^{15}\epsilon_{fix}$. The results also suggest potential compensatory mechanisms of in vivo physiology to maintain high efficiency substrate-

cofactor interaction despite mutation (Supplementary Results S2.1).

Wild-type V-nitrogenase $^{15}\epsilon_{fix}$: high efficiency catalysis nearing that of wild-type Mo-nitrogenase

Our analyses of $^{15}\epsilon_{fix}$ indicate high N_2 use efficiency, f_{used}, for all nitrogenases, including the V-isoform ($f_{used} > 0.8$ for V-only vs. >0.9 for WT, Fig. 4d). This provides strong support for the N_2 Channel Hypothesis for the in vivo $^{15}\epsilon_{fix}$ being small compared to the fractionation by the chemical KIE . Nevertheless, the Cofactor Activation hypothesis could explain the small-scale $^{15}\epsilon_{fix}$ variations between isoforms. Lower electron-use efficiency of the V-nitrogenase cofactor (21) would cause an increase in $^{15}\epsilon_{fix}$ as well as decreases in N_2:H_2 ratio and growth rate (Fig. 3a, Data S1 and S2). But links between these parameters are hard to quantify experimentally because there are multiple H_2 evolving steps before N_2 binding (e.g. E_2 and E_4 decay, Fig. 1b, see Supplementary Discussion S3.2). Alternatively, higher $^{15}\epsilon_{fix}$ values for the V-isoform could reflect isoform-specific KIE_{diff} variation.

Both scenarios are compatible with the relative stability of V-only $^{15}\epsilon_{fix}$ to physiological changes (5.8–6.6‰, Supplementary Results S2.2). The data could reflect the same degree of KIE_{cat} expression across conditions (Cofactor Activation hypothesis) or the exclusive expression of the isoform-specific KIE_{diff} (N_2 Channel hypothesis). Further validation of the specific causes of the consistently high V-only $^{15}\epsilon_{fix}$ requires clarification on how physiology and enzyme structure constrain electron use efficiency for NH_3-production and the expression of KIE_{diff} for nitrogenase isoforms.

Discussion

Using isotope modeling and laboratory experiments, we find that cellular $^{15}\epsilon_{fix}$ values in the unicellular model diazotroph *A. vinelandii* directly reflect the isotope effects of the nitrogenase enzyme, in particular, the KIE of N_2 diffusion within the enzyme. These N isotope dynamics can be explained by efficient N_2-cofactor interactions driven by a high reactivity cofactor. Data from mutants indicate how enzyme active site protein structure (particularly key amino acid residues for optimal N_2 access and positioning) promotes substrate–cofactor interactions, affecting catalytic efficiency, which is quantified by $^{15}\epsilon_{fix}$. However, enzymatic $^{15}\epsilon_{fix}$ of diazotrophs inhabiting biophysically complex environments (e.g. multicellular, living in nodules, mats) may be masked by a limited external N_2 reservoir, such that organism-scale $^{15}\epsilon_{fix}$ shifts toward the KIE of external N_2 transport (Fig. 1b). Thus far, however, studies indicate relatively minor effects of external N_2 availability (~2‰) (8, 9). In addition, studies that infer $^{15}\epsilon_{fix}$ based on the $\delta^{15}N$ of particulate organic N should consider the isotopic effects of fixed N excretion, which can cause a few per mil offset from the true $^{15}\epsilon_{fix}$ based on the entire newly fixed N pool (23).

Our mechanistic findings should be broadly applicable since strong conservation of cellular $^{15}\epsilon_{fix}$ values for each natural nitrogenase isoform across diazotroph lineages (1–3‰ for Mo-, 5–6‰ for V-, and 7–8‰ for Fe-isoforms; Data S2 and references therein) indicates a minor lineage effect on $^{15}\epsilon_{fix}$. Consistent with this, key functional amino acid residues in modern nitrogenase are largely invariant (Fig. S2b). Moreover, none of the active site mutations examined here, including the α-70 gatekeeper associated with large $^{15}\epsilon_{fix}$ variability, exist in these natural nitrogenases (Fig. S2b). Thus, all extant nitrogenases likely maintain high catalytic efficiency ($f_{used} > \sim 0.8$) across different physiological contexts, which likely derives from structural optimization of the active site for chemical steps relative to the diffusional supply of N_2.

Our mechanistic findings on BNF $^{15}\epsilon_{fix}$ have implications for multiple research areas. Most notably, identification of the in vivo rate-limiting step of N_2 reduction enables new insights into the coevolution of enzyme structure–function with cellular physiology and environmental changes in the past and present.

Nitrogenase functional evolution and N cycle studies

Lower values of measured $^{15}\epsilon_{fix}$ (0 to 17‰, Data S2) relative to the fractionation (27±10 ‰, see Results) from the expected chemical KIE (1.017 to 1.037), which reflect high catalytic efficiency, result from N_2 diffusion limitation within the optimized active site of nitrogenase (6, 16, 43). The near complete substrate use for Mo-nitrogenase is consistent with its earlier evolution than alternative nitrogenases (14, 19, 20, 79, 80). This earlier evolution would have provided additional time for structural optimization towards higher substrate use efficiency, possibly to keep up with higher N demand induced by the increasing biomass of Earth's ecosystems. Phylogenetic studies suggested the structural optimization of Mo-nitrogenase may have happened after the Great Oxidation Event (GOE), when the rise of persistent oxidized environments augmented bioavailability of Mo, after which the Mo uptake and cofactor maturation and insertion had sufficient time to be optimized by genomic evolution (81).

The functional characteristics of nitrogenase are sensitive to its substrate channel architecture beyond the active site (7, 58–60, 73, 82). Given this, why does the N_2 substrate channel not allow additional N_2 transport to maximize NH_3 production? For example, a higher NH_3 production rate could potentially be achieved with a higher gas flux channel despite lower substrate use efficiency in the active site. However, this channel architecture could also affect diffusion of nontarget molecules like molecular oxygen, which irreversibly damages the cofactor (83, 84). We suggest that the evolution of nitrogenase towards diffusion limitation (low $^{15}\epsilon_{fix}$) was caused or encouraged by environmental oxygen, the concentration of which varied drastically over Earth history (82, 85). Nitrogenase with a reactive cofactor and high gas transport capacity substrate channel (exhibiting higher $^{15}\epsilon_{fix}$) may have been prevalent prior to the rise of atmospheric O_2. Our isotopic analyses strongly support the post-GOE emergence of the modern Mo-nitrogenase structure (14, 19, 20, 79, 80), complementing the above-mentioned phylogenetic proposal about post-GOE evolution of molybdenum uptake system and cofactor maturase genes (81). Additionally, an active site with high N_2 use efficiency shaped by O_2 would support enzyme function as a nitrogenase vs. hydrogenase. This would increase the fitness of diazotrophs in an oxygenated world with low fixed N availability.

Our analyses confirm that cellular $^{15}\epsilon_{fix}$ is a robust indicator of natural isozyme types in modern environments. But the results imply that isoform $^{15}\epsilon_{fix}$ values could have varied over geological time scales (e.g. ancient enzymes prior to the GOE with higher $^{15}\epsilon_{fix}$), suggesting $^{15}\epsilon_{fix}$-based inferences of N cycle linkage to environmental redox state and trace metal availability require re-examination (14, 16, 86, 87). Re-evaluation of the C isotope record has also been suggested based on potential differences in C isotope fractionation between modern and ancient Rubisco (88). Thus, N isotope studies of historical BNF and its role in ancient N cycling, particularly over periods of environmental oxygen shift,

would benefit from a holistic assessment of $^{15}\epsilon_{fix}$ (including effects of structure–function, cellular, and environmental context such as local variations in N_2, O_2, electron availability, and CO_2 (89, 90)).

A broader assessment of $^{15}\epsilon_{fix}$ variability and the potential impacts of diagenesis of signal preservation would help reconcile our results, which imply early nitrogenases produced organic N with very negative $\delta^{15}N$ values, with the predominance of $\delta^{15}N$ values of 0±2‰ and higher for Archean sedimentary rocks (91). The mechanisms identified in this study can guide such assessments and may also inform interpretation of the isotopic records of other biogeochemical processes (Supplementary Discussion S3.4) (30, 34, 65, 88).

Biochemistry, physiology, and chemistry of nitrogen fixation

While our $^{15}\epsilon_{fix}$ study focuses on in vivo nitrogenase kinetics, N isotopic approaches may also be useful in studies of in vitro nitrogenase mechanism complementing existing biochemical studies. For example, in vitro $^{15}\epsilon_{fix}$ can help constrain whether the rate-limiting step shifts from N≡N bond-breaking step to N_2 diffusion under high electron condition (37). By elucidating $^{15}\epsilon_{fix}$ sensitivities to biochemical conditions, these studies can help constrain relationships between electron and substrate use efficiency to explain in vivo V-isoform $^{15}\epsilon_{fix}$ (Supplementary Discussion S3.2). Additionally, the role of substrate use efficiency under different physiological conditions (e.g. nonsteady state) could be evaluated through measurements of $^{15}\epsilon_{fix}$. Finally, stable isotopic methods can also aid in understanding carbon compound reduction by nitrogenases (acetylene reduction isotope effect, Supplementary Discussion S3.3) and guide efforts to improve chemical N_2 fixation for industry and agriculture (92, 93).

Conclusions

Our study demonstrates that in vivo BNF reaction by nitrogenase is rate limited by enzymatic N_2 diffusion. Further elucidation of the mechanisms and principles underlying nitrogenase function will advance our understanding of the evolutionary trajectory of nitrogenase structure to a so-called "perfect enzyme," which we suggest is associated with atmospheric oxygenation in Earth history. Thus, nitrogenase nitrogen isotope dynamics could exemplify the effects of global environmental redox change on enzyme structural evolution. In addition, a better mechanistic understanding of nitrogenase reaction kinetics achieved with N stable isotopes may facilitate the development of more environmentally sustainable methods of N_2 fixation.

Materials and methods

Bacterial cultures

We employed 13 different *A. vinelandii* DJ strains: WT and V-only (DJ995 and CA11.70) (62, 94, 95) and the 11 DJ strains (46, 49, 50, 96–98) with *nif* gene mutations provided by the Dean laboratory at the University of Virginia (Table 1). Each strain was grown in aerobic batch cultures in Nunc flask containing 50 mL of a modified liquid Burk's medium with replete Mo or V concentrations (100 nM) at 200 rpm and 30°C (Figs. S3–S6) (62). Chemostat experiments were performed on the WT, V-only, and two *nif* mutant strains, Na1 and Na2. Dilution rates were very slow or slow (0.6 or 2 d^{-1}) relative to batch culture growth rates. The wild type, V-only, and mutant strains were grown and measured in ≥4 biological replicates. Cell growth was monitored by $OD_{620\ nm}$ measurements. Details on *nif* mutant strain selection, media recipe, batch cultures, chemostat setup and operation, growth measurements, and cell sampling are in Supplementary Materials and methods.

Protein quantification

Total protein content in frozen bacterial cell pellets were analyzed by BCA methods using Pierce BCA Protein Assay Kits (Thermo Fisher Scientific, Part No. 23225). For *NifDKH* quantification, 0.2 mg of total protein sample was analyzed by Western blot. *NifDK* antibody was provided by the Dean laboratory, and *NifH* antibody from Agrisera. For quantitative Western blot, we used purified *NifDK* and *NifH* provided from the Dean Laboratory as a standard. BCA analysis and Western blots were performed at RayBiotech, GA (https://www.raybiotech.com). We note enzymatic N_2 diffusion western blots may potentially overestimate %*NifDK* and thus underestimate specific activity of some strains because of incomplete removal of proteins stuck to alginate coating during wash steps.

N_2 fixation rate estimation

N_2 fixation rate per cell was estimated by multiplying growth rate (μ) and total particulate and dissolved N per cell measured by elemental isotope ratio mass spectrometry. This rate is constant in chemostat. In batch culture, we used the N concentration measured at mid-exponential phase. Specific activity was calculated as N_2 fixation rate per cell divided by total *NifDK* concentration per cell.

N quantification and ^{15}N analysis

Sample $^{15}N/^{14}N$ isotopic content is defined as:

$$\delta^{15}N_{sample} = [(^{15}N/^{14}N)_{sample}/(^{15}N/^{14}N)_{air\ N2} - 1] \times 1,000 \text{ in permil (‰)}.$$

The observed isotopic fractionation for BNF ($^{15}\epsilon_{fix}$) is measured as the difference in $\delta^{15}N$ between dissolved N_2 and newly fixed N:

$$^{15}\epsilon_{fix} = \delta^{15}N_{dissolved\ N2} - \delta^{15}N_{newly\ fixed\ N} \text{ where } \delta^{15}N_{dissolved\ N2} = 0.7‰ (12).$$

Newly fixed N is either stored in cellular biomass or excreted into the medium. Supernatant N comprises excreted N and EDTA. EDTA is metal chelator in growth medium, contains the 2 N atoms per molecule, and cannot be used as fixed N source for growth. We estimated $\delta^{15}N$ of newly fixed N ($\delta^{15}N_{newly\ fixed\ N}$) in culture samples by separating them into three or two different N fractions: separated cell biomass pellet, supernatant, fresh medium fractions (method A) or as a combined cell and supernatant fraction and the fresh medium fraction (method B). Method B was less laborious than method A and yielded the statistically similar sample $^{15}\epsilon_{fix}$ values as method A. See details in the Supplementary Materials and methods.

Isotope modeling: nitrogenase reaction scheme

We developed a steady state N isotope model of the cellular nitrogenase reaction based on the Thorneley–Lowe reaction scheme (29, 35) (see Eqs. (1)–(3)). First, to model N_2 transport, we combined the external cellular N_2 diffusion (Fig. 1b green box) step with internal N_2 diffusion from the enzyme surface to its active site (Fig. 1b orange) since we could not constrain the KIE and EIE of individual steps, particularly those in nitrogenase. Second, we combined N_2 binding and the N≡N bond breaking into a single step

(Fig. 1b, N_2 catalysis box), as most biochemical studies of the mechanism indicate these steps are kinetically inseparable (see Supplementary Materials and methods S1.7) (6, 36, 37). Third, we did not include N_2 unbinding at the E_4 cofactor (oxidation of 2N2H into N≡N and consequent release of N≡N from cofactor; leftward arrow from E_4(2N2H) in Fig. 1b) or any further reductions past N≡N bond breaking (from E_4-2N2H to E_0 and $2NH_3$, Fig 1b) within the model since N_2 unbinding has only been detected in vitro at high H_2 partial pressure (0.7 atm) (39). Irreversible N≡N catalysis in cellular environments is supported by our examination of N isotope effects (Supplementary Materials and methods S1.8). Possible KIE and EIE values were estimated using biochemical observation and physical chemical calculations (1 to 1.0068 for KIE_{diff}, 1.017 to 1.037 for KIE_{cat}, see Results).

Model fitting to measured $^{15}\epsilon_{fix}$

Model solutions for the KIE_{diff}, KIE_{cat}, and f ratios (see Eqs. (1–3)) matching the measured $^{15}\epsilon_{fix}$ values were determined by grid search (R Code S2). The $^{15}\epsilon_{fix}$ measurements comprise data from this study (13 batch cultures, 7 chemostat cultures) and a prior study (an in vitro WT Mo-nitrogenase measurement (26)). We searched for combinations of the KIE_{diff}, KIE_{cat}, and f parameters that minimized the difference between the estimated and the measured α_{fix} values within <0.0005 (i.e. $\Delta^{15}\varepsilon_{fix} = |\text{Predicted } ^{15}\varepsilon_{fix} - \text{Measured } ^{15}\varepsilon_{fix}| < 0.5‰$). The searching interval was 0.0001 for KIE_{diff}, 0.001 for KIE_{cat}, 0.01 for f_{used}, over ranges of 1 to 1.0068 for KIE_{diff}, 1.017 to 1.0037 for KIE_{cat}, and 0 to 1 for f_{used}. KIE values were assumed to be constant for the same enzyme regardless of reaction/culture condition, i.e. only f could vary.

Acknowledgments

We thank Dr Dennis R. Dean and Valerie L. Cash (Virginia Polytechnic Institute and State University) for generously sharing *Azotobacter nif*-mutant strains; Drs Sergey Oleynik, Jessica Lueders-Dumont, Katja E. Luxem (Princeton University) for technical help with NOx box, denitrifier method, and EA-IRMS measurements.

Supplementary Material

Supplementary material is available at *PNAS Nexus* online.

Funding

This work was supported by National Aeronautics and Space Administration Award 80NSSC17K0667 (to X.Z. and S.H.K.), the High Meadows Environmental Institute Carbon Mitigation Initiative at Princeton University (to X.Z.), the Simons Foundation (Early Career Fellowship in Marine Microbiology Award 622944 to X.Z.), and Kwanjeong Educational Foundation Award 17AmB24D (to E.H.).

Author Contributions

E.H., S.H.K., and X.Z. designed research; E.H., A.E.M., and X.E.A. performed research; S.H.K, D.M.S., and X.Z. contributed new reagents/analytic tools; E.H., S.H.K., and X.Z. analyzed data; E.H., S.H.K., and X.Z. wrote the article with inputs from all authors.

Data Availability

The experimental data and R code used in this study are available at https://github.com/ehan-geobio/MS1-BNF-d15N. See Supplementary material for the data and code legend.

References

1 Zhang X, Ward BB, Sigman DM. 2020. Global nitrogen cycle: critical enzymes, organisms, and processes for nitrogen budgets and dynamics. *Chem Rev*. 120:5308–5351.
2 Harris DF, *et al*. 2019. Mo-, V-, and Fe-nitrogenases use a universal eight-electron reductive-elimination mechanism to achieve N_2 reduction. *Biochemistry*. 58:3293–3301.
3 Luxem KE, Nguyen AJ, Zhang X. 2022. Biohydrogen production relationship to biomass composition, growth, temperature and nitrogenase isoform in the anaerobic photoheterotrophic diazotroph *Rhodopseudomonas palustris*. *Int J Hydrogen Energy*. 47: 28399–28409.
4 Simpson FB, Burris RH. 1984. A nitrogen pressure of 50 atmospheres does not prevent evolution of hydrogen by nitrogenase. *Science*. 224:1095–1097.
5 Ertl G. 2008. Reactions at surfaces: from atoms to complexity (nobel lecture). *Angew Chem Int Ed Engl*. 47:3524–3535.
6 Hoffman BM, Lukoyanov DA, Dean DR, Seefeldt LC. 2013. Nitrogenase: a draft mechanism. *Acc Chem Res*. 46:587–595.
7 Kim J, Rees DC. 1994. Nitrogenase and biological nitrogen fixation. *Biochemistry*. 33:389–397.
8 Unkovich M. 2013. Isotope discrimination provides new insight into biological nitrogen fixation. *New Phytol*. 198:643–646.
9 Silverman SN, Kopf SH, Bebout BM, Gordon R, Som SM. 2019. Morphological and isotopic changes of heterocystous cyanobacteria in response to N_2 partial pressure. *Geobiology*. 17:60–75.
10 Bennett LT, Jacobson MR, Dean DR. 1988. Isolation, sequencing, and mutagenesis of the *nifF* gene encoding flavodoxin from *Azotobacter vinelandii*. *J Biol Chem*. 263:1364–1369.
11 O'leary MH. 1981. Carbon isotope fractionation in plants. *Phytochemistry*. 20:553–567.
12 Sigman DM, Fripiat F. Nitrogen isotopes in the ocean. In: *Encyclopedia of ocean sciences*. 3rd ed. Oxford: Academic Press, 2019. p. 263–278.
13 Marconi D, *et al*. 2017. Tropical dominance of N_2 fixation in the North Atlantic Ocean. *Global Biogeochem Cycles*. 31:1608–1623.
14 Stüeken EE, Buick R, Guy BM, Koehler MC. 2015. Isotopic evidence for biological nitrogen fixation by molybdenum-nitrogenase from 3.2 Gyr. *Nature*. 520:666–669.
15 Klots CE, Benson BB. 1963. Isotope effect in the solution of oxygen and nitrogen in distilled water. *J Chem Phys*. 38:890–892.
16 Zhang X, Sigman DM, Morel FMM, Kraepiel AML. 2014. Nitrogen isotope fractionation by alternative nitrogenases and past ocean anoxia. *Proc Natl Acad Sci U S A*. 111:4782–4787.
17 Burgess BK, Lowe DJ. 1996. Mechanism of molybdenum nitrogenase. *Chem Rev*. 96:2983–3012.
18 Eady RR. 2003. Current status of structure function relationships of vanadium nitrogenase. *Coord Chem Rev*. 237:23–30.
19 Boyd ES, Hamilton TL, Peters JW. 2011. An alternative path for the evolution of biological nitrogen fixation. *Front Microbiol*. 2:205.
20 Boyd ES, *et al*. 2011. A late methanogen origin for molybdenum-dependent nitrogenase. *Geobiology*. 9:221–232.
21 Einsle O. 2023. On the shoulders of giants—reaching for nitrogenase. *Molecules*. 28:7959.
22 Nishizawa M, Miyazaki J, Makabe A, Koba K, Takai K. 2014. Physiological and isotopic characteristics of nitrogen fixation

by hyperthermophilic methanogens: key insights into nitrogen anabolism of the microbial communities in Archean hydrothermal systems. *Geochim Cosmochim Acta*. 138:117–135.
23 McRose DL, *et al.* 2019. Effect of iron limitation on the isotopic composition of cellular and released fixed nitrogen in *Azotobacter vinelandii*. *Geochim Cosmochim Acta*. 244:12–23.
24 Harwood CS. 2020. Iron-only and vanadium nitrogenases: fail-safe enzymes or something more? *Annu Rev Microbiol*. 74:247–266.
25 Rowell P, James W, Smith WL, Handley LL, Scrimgeour CM. 1998. ^{15}N discrimination in molybdenum-and vanadium-grown N_2-fixing *Anabaena variabilis* and *Azotobacter vinelandii*. *Soil Biol Biochem*. 30:2177–2180.
26 Sra AK, *et al.* 2004. Competitive ^{15}N kinetic isotope effects of nitrogenase-catalyzed dinitrogen reduction. *J Am Chem Soc*. 126: 12768–12769.
27 Hoering TC, Ford HT. 1960. The isotope effect in the fixation of nitrogen by *Azotobacter*. *J Am Chem Soc*. 82:376–378.
28 Hayes JM. 2001. Fractionation of carbon and hydrogen isotopes in biosynthetic processes. *Stable Isotope Geochem*. 43:225–278.
29 Seefeldt LC, Hoffman BM, Dean DR. 2009. Mechanism of Mo-dependent nitrogenase. *Annu Rev Biochem*. 78:701–722.
30 Karsh KL, Granger J, Kritee K, Sigman DM. 2012. Eukaryotic assimilatory nitrate reductase fractionates N and O isotopes with a ratio near unity. *Environ Sci Technol*. 46:5727–5735.
31 Mariotti A, *et al.* 1982. Nitrogen isotope fractionation associated with nitrate reductase activity and uptake of NO_3^- by Pearl Millet. *Plant Physiol*. 69:880–884.
32 Emerson S, Stump C, Wilbur D, Quay P. 1999. Accurate measurement of O_2, N_2, and Ar gases in water and the solubility of N_2. *Mar Chem*. 64:337–347.
33 Ono S, Sim MS, Bosak T. 2014. Predictive isotope model connects microbes in culture and nature. *Proc Natl Acad Sci U S A*. 111: 18102–18103.
34 Wilkes EB, Pearson A. 2019. A general model for carbon isotopes in red-lineage phytoplankton: interplay between unidirectional processes and fractionation by RubisCO. *Geochim Cosmochim Acta*. 265:163–181.
35 Thorneley RNF, Lowe DJ. 1983. Nitrogenase of *Klebsiella pneumoniae* kinetics of the dissociation of oxidized iron protein from molybdenum-iron protein: identification of the rate-limiting step for substrate reduction. *Biochem J*. 215:393–403.
36 Raugei S, Seefeldt LC, Hoffman BM. 2018. Critical computational analysis illuminates the reductive-elimination mechanism that activates nitrogenase for N_2 reduction. *Proc Natl Acad Sci U S A*. 115:E10521–E10530.
37 Harris DF, Badalyan A, Seefeldt LC. 2022. Mechanistic insights into nitrogenase FeMo-cofactor catalysis through a steady-state kinetic model. *Biochemistry*. 61:2131–2137.
38 Lukoyanov D, Barney BM, Dean DR, Seefeldt LC, Hoffman BM. 2007. Connecting nitrogenase intermediates with the kinetic scheme for N2 reduction by a relaxation protocol and identification of the N_2 binding state. *Proc Natl Acad Sci U S A*. 104: 1451–1455.
39 Yang ZY, *et al.* 2013. On reversible H_2 loss upon N_2 binding to FeMo-cofactor of nitrogenase. *Proc Natl Acad Sci U S A*. 110: 16327–16332.
40 Kritee K, *et al.* 2012. Reduced isotope fractionation by denitrification under conditions relevant to the ocean. *Geochim Cosmochim Acta*. 92:243–259.
41 Bar-Even A, *et al.* 2011. The moderately efficient enzyme: evolutionary and physicochemical trends shaping enzyme parameters. *Biochemistry*. 50:4402–4410.
42 Bar-Even A, Milo R, Noor E, Tawfik DS. 2015. The moderately efficient enzyme: futile encounters and enzyme floppiness. *Biochemistry*. 54:4969–4977.
43 Knowles JR, Albery WJ. 1977. Perfection in enzyme catalysis: the energetics of triosephosphate isomerase. *Acc Chem Res*. 10: 105–111.
44 Yang Z-Y, *et al.* 2016. Pi release is rate limiting step for nase catalysis with flavodoxin reductant. *Biochemistry*. 55:3625–3635.
45 Seefeldt LC. 1994. Docking of nitrogenase iron-and molybdenum-iron proteins for electron transfer and MgATP hydrolysis: the role of arginine 140 and lysine 143 of the *Azotobacter vinelandii* iron protein. *Protein Sci*. 3:2073–2081.
46 Brigle KE, *et al.* 1987. Site-directed mutagenesis of the nitrogenase MoFe protein of *Azotobacter vinelandii*. *Proc Natl Acad Sci U S A*. 84:7066–7069.
47 Barney BM, *et al.* 2005. Trapping a hydrazine reduction intermediate on the nitrogenase active site. *Biochemistry*. 44: 8030–8037.
48 Barney BM, Igarashi RY, Dos Santos PC, Dean DR, Seefeldt LC. 2004. Substrate interaction at an iron-sulfur face of the FeMo-cofactor during nitrogenase catalysis. *J Biol Chem*. 279: 53621–53624.
49 Christiansen J, Seefeldt LC, Dean DR. 2000. Competitive substrate and inhibitor interactions at the physiologically relevant active site of nitrogenase. *J Biol Chem*. 275:36104–36107.
50 Christiansen J, Chan JM, Seefeldt LC, Dean DR. 2000. The role of the MoFe protein α-125Phe and β-125Phe residues in *Azotobacter vinelandii* MoFe protein–Fe protein interaction. *J Inorg Biochem*. 80:195–204.
51 Rivera-Ortiz JM, Burris RH. 1975. Interactions among substrates and inhibitors of nitrogenase. *J Bacteriol*. 123:537–545.
52 DeLano WL. 2002. Pymol: an open-source molecular graphics tool. *CCP4 Newsl Protein Crystallogr*. 40:82–92.
53 Einsle O, *et al.* 2002. Nitrogenase MoFe-protein at 1.16 Å resolution: a central ligand in the FeMo-cofactor. *Science*. 297: 1696–1700.
54 Sarma R, *et al.* 2010. Insights into substrate binding at FeMo-cofactor in nitrogenase from the structure of an α-70Ile MoFe protein variant. *J Inorg Biochem*. 104:385–389.
55 Sippel D, Einsle O. 2017. The structure of vanadium nitrogenase reveals an unusual bridging ligand. *Nat Chem Biol*. 13:956–960.
56 Muraki N, *et al.* 2010. X-ray crystal structure of the light-independent protochlorophyllide reductase. *Nature*. 465: 110–114.
57 Kaiser JT, Hu Y, Wiig JA, Rees DC, Ribbe MW. 2011. Structure of precursor-bound *NifEN*: a nitrogenase FeMo cofactor maturase/insertase. *Science*. 331:91–94.
58 Morrison CN, Hoy JA, Zhang L, Einsle O, Rees DC. 2015. Substrate pathways in the nitrogenase MoFe protein by experimental identification of small molecule binding sites. *Biochemistry*. 54: 2052–2060.
59 Kim J, Rees DC. 1992. Crystallographic structure and functional implications of the nitrogenase molybdenum–iron protein from *Azotobacter vinelandii*. *Nature*. 360:553–560.
60 Howard JB, Kechris KJ, Rees DC, Glazer AN. 2013. Multiple amino acid sequence alignment nitrogenase component 1: insights into phylogenetics and structure-function relationships. *PLoS One*. 8: e72751.
61 Oelze J. 2000. Respiratory protection of nitrogenase in Azotobacter species: is a widely held hypothesis unequivocally supported by experimental evidence? *FEMS Microbiol Rev*. 24: 321–333.

62 Bellenger JP, Wichard T, Xu Y, Kraepiel AML. 2011. Essential metals for nitrogen fixation in a free-living N_2-fixing bacterium: chelation, homeostasis and high use efficiency. *Environ Microbiol*. 13: 1395–1411.

63 Kuhla J, Oelze J. 1988. Dependence of nitrogenase switch-off upon oxygen stress on the nitrogenase activity in *Azotobacter vinelandii*. *J Bacteriol*. 170:5325–5329.

64 Inomura K, Bragg J, Follows MJ. 2017. A quantitative analysis of the direct and indirect costs of nitrogen fixation: a model based on *Azotobacter vinelandii*. *ISME J*. 11:166–175.

65 Wing BA, Halevy I. 2014. Intracellular metabolite levels shape sulfur isotope fractionation during microbial sulfate respiration. *Proc Natl Acad Sci U S A*. 111:18116–18125.

66 Mason EA, Marrero TR. The diffusion of atoms and molecules. In: *Advances in atomic and molecular physics*. Oxford: Academic Press, 1970. p. 155–232.

67 Herzberg G, Crawford BL Jr. 1946. Infrared and Raman spectra of polyatomic molecules. *J Phys Chem*. 50(3):288–288.

68 Herzberg G. 1950. Rotation-vibration spectra of diatomic and simple polyatomic molecules with long absorbing paths VI. The spectrum of nitrous oxide (N_2O) below 1.2μ. *J Chem Phys*. 18: 1551–1561.

69 Haschke S, *et al*. 2018. Direct oxygen isotope effect identifies the rate-determining step of electrocatalytic OER at an oxidic surface. *Nat Commun*. 9:4565.

70 Tcherkez GGB, Farquhar GD, Andrews TJ. 2006. Despite slow catalysis and confused substrate specificity, all ribulose bisphosphate carboxylases may be nearly perfectly optimized. *Proc Natl Acad Sci U S A*. 103:7246–7251.

71 Craig NC, Levin IW. 1979. Vibrational assignment and potential function for trans-diazene (diimide): predictions for cis-diazene. *J Chem Phys*. 71:400–407.

72 Richet P, Bottinga Y, Javoy M. 1977. A review of hydrogen, carbon, nitrogen, oxygen, sulphur, and chlorine stable isotope fractionation among gaseous molecules. *Annu Rev Earth Planet Sci*. 5: 65–110.

73 Igarashi RY, Seefeldt LC. 2003. Nitrogen fixation: the mechanism of the Mo-dependent nitrogenase. *Crit Rev Biochem Mol Biol*. 38: 351–384.

74 Lee HI, *et al*. 2004. An organometallic intermediate during alkyne reduction by nitrogenase. *J Am Chem Soc*. 126:9563–9569.

75 Lukoyanov DA, *et al*. 2023. A conformational equilibrium in the nitrogenase MoFe protein with an α-V70I amino acid substitution illuminates the mechanism of H_2 formation. *Faraday Discuss*. 243: 231–252.

76 Benton PMC, *et al*. 2001. Interaction of acetylene and cyanide with the resting state of nitrogenase α-96-substituted MoFe proteins. *Biochemistry*. 40:13816–13825.

77 Plunkett MH, Knutson CM, Barney BM. 2020. Key factors affecting ammonium production by an *Azotobacter vinelandii* strain deregulated for biological nitrogen fixation. *Microb Cell Fact*. 19:107.

78 Knutson CM, Plunkett MH, Liming RA, Barney BM. 2018. Efforts toward optimization of aerobic biohydrogen reveal details of secondary regulation of biological nitrogen fixation by nitrogenous compounds in *Azotobacter vinelandii*. *Appl Microbiol Biotechnol*. 102:10315–10325.

79 Garcia AK, Kolaczkowski B, Kaçar B. 2022. Reconstruction of nitrogenase predecessors suggests origin from maturase-like proteins. *Genome Biol Evol*. 14:evac031.

80 Garcia AK, *et al*. 2023. Nitrogenase resurrection and the evolution of a singular enzymatic mechanism. *Elife*. 12:e85003.

81 Lee CC, Górecki K, Stang M, Ribbe MW, Hu Y. 2024. Cofactor maturase NifEN: a prototype ancient nitrogenase? *Sci Adv*. 10: eado6169.

82 Cadoux C, *et al*. 2023. The mononuclear metal-binding site of Mo-nitrogenase is not required for activity. *JACS Au*. 3:2993–2999.

83 Lee SC, Lo W, Holm RH. 2014. Developments in the biomimetic chemistry of cubane-type and higher nuclearity iron-sulfur clusters. *Chem Rev*. 114:3579–3600.

84 Gallon JR. 1981. The oxygen sensitivity of nitrogenase: a problem for biochemists and micro-organisms. *Trends Biochem Sci*. 6:19–23.

85 Berman-Frank I, Cullen JT, Shaked Y, Sherrell RM, Falkowski PG. 2001. Iron availability, cellular iron quotas, and nitrogen fixation in Trichodesmium. *Limnol Oceanogr*. 46:1249–1260.

86 Philippi M, *et al*. 2021. Purple sulfur bacteria fix N_2 via molybdenum-nitrogenase in a low molybdenum Proterozoic ocean analogue. *Nat Commun*. 12:4774.

87 Anbar AD, Knoll AH. 2002. Proterozoic ocean chemistry and evolution: a bioinorganic bridge? *Science*. 297:1137–1142.

88 Wang RZ, *et al*. 2023. Carbon isotope fractionation by an ancestral rubisco suggests that biological proxies for CO_2 through geologic time should be reevaluated. *Proc Natl Acad Sci U S A*. 120: e2300466120.

89 Nicola W, E SE, Thorsten B, M GM. 2024. Exploring the influence of atmospheric CO_2 and O_2 levels on the utility of nitrogen isotopes as proxy for biological N_2 fixation. *Appl Environ Microbiol*. 90:e00574-24.

90 Wen Z, *et al*. 2024. Effects of CO_2 on the nitrogen isotopic composition of marine diazotrophic cyanobacteria. *Geophys Res Lett*. 51: e2024GL110599.

91 Stüeken EE, Kipp MA, Koehler MC, Buick R. 2016. The evolution of Earth's biogeochemical nitrogen cycle. *Earth Sci Rev*. 160:220–239.

92 Seefeldt LC, Yang ZY, Duval S, Dean DR. 2013. Nitrogenase reduction of carbon-containing compounds. *Biochim Biophys Acta Bioenerg*. 1827:1102–1111.

93 Zhang X, *et al*. 2016. Alternative nitrogenase activity in the environment and nitrogen cycle implications. *Biogeochemistry*. 127: 189–198.

94 Joerger RD, *et al*. 1990. Genes for nitrogenase 2 of *Azotobacter vinelandii*. *J Bacteriol*. 172:3400–3408.

95 Premakumar R, Jacobitz S, Ricke SC, Bishop PE. 1996. Phenotypic characterization of a tungsten-tolerant mutant of *Azotobacter vinelandii*. *J Bacteriol*. 178:691–696.

96 Dilworth MJ. 1998. Effects on substrate reduction of substitution of histidine-195 by glutamine in the α-subunit of the MoFe protein of *Azotobacter vinelandii* nitrogenase. *Biochemistry*. 37: 17495–17505.

97 Fisher K, Dilworth MJ, Newton WE. 2000. Differential effects on N_2 binding and reduction, HD formation, and azide reduction with α-195(His)- and α-191(Gln)-substituted MoFe proteins of *Azotobacter vinelandii* nitrogenase. *Biochemistry*. 39:15570–15577.

98 Fisher K, Dilworth MJ, Kim CH, Newton WE. 2000. *Azotobacter vinelandii* nitrogenases containing altered MoFe proteins with substitutions in the FeMo-cofactor environment: effects on the catalyzed reduction of acetylene and ethylene. *Biochemistry*. 39: 2970–2979.